Recent Development of Low-dose X-ray Cone-beam Computed Tomography

Jing Wang*,1,2, Zhengrong Liang[3], Hongbing Lu[4], and Lei Xing[1]

[1]*Department of Radiation Oncology, Stanford University School of Medicine, Stanford, CA 94305, USA*

[2]*Department of Radiation Oncology, University of Texas Southwestern Medical Center, Dallas, TX 75390, USA*

[3]*Departments of Radiology and Computer Science, Stony Brook University, Stony Brook, NY 11794, USA*

[4]*Department of Biomedical Engineering/Computer Application, Fourth Military Medical University, Xi'an, Shaanxi 710032, China*

Abstract: Cone-beam computed tomography (CBCT) is an emerging medical imaging modality used for various clinical applications. However, radiation dose to patients is a major limiting factor for its utility in some applications such as daily patient setup and future adaptive therapy in radiotherapy. In this article, we summarize recent development for dose reduction in CBCT. In particular, we discuss several noise reduction strategies for low-dose CBCT with a low mAs protocol.

I. INTRODUCTION

With the development of large area flat-panel detectors, cone-beam computed tomography (CBCT) has become an emerging medical imaging modality and been widely used for various clinical applications such as for breast imaging and image-guided radiation therapy (IGRT) [1-28]. Compared with conventional digital mammography, CBCT breast imaging provides volumetric information which potentially can improve lesion detection accuracy with increased radiation dose. In radiation therapy, integration of the CBCT with a linear accelerator makes it possible to acquire a high-resolution volumetric image of a patient at a treatment position. There is growing interest in using on-board CBCT for a patient treatment position setup and dose reconstruction in radiotherapy [8, 29-31]. The repeated use of CBCT during a course of radiotherapy treatment has raised concerns of extra radiation dose delivered to patients [32-35]. For example, it has been reported [34] that the dose delivered from Varian's CBCT system with current clinical protocols for pelvic area is more than 3 cGy for central tissue, about 5 cGy for most of the peripheral tissues and 11 cGy to femoral head. If CBCT is used daily for patient setup, the total CBCT imaging dose delivered to patient could be extremely high in a course of intensity-modulated radiation therapy (IMRT) treatment. The extra radiation exposure to normal tissue during kV-CBCT will significantly increase the probability of stochastic risk of inducing cancer and genetic defects. The CBCT dose needs to be minimized to fully realize its advantages in these clinical applications.

CBCT imaging dose is affected by many factors including tube potential (kVp), tube current and exposure time (mAs), beam quality, beam collimation, etc. Dose reduction for CBCT can be achieved via X-ray beam collimation/filtration or using a low mAs protocol. In this article, we summarize recent development of dose reduction techniques for CBCT including different design of beam collimators, iterative image reconstruction algorithms for CBCT based on undersampled projection views, and noise reduction techniques for low-dose CBCT with a low mAs protocol.

II. COLLIMATOR-BASED METHODS

CBCT imaging dose can be reduced by using X-ray filters or collimators. In commercial scanners, two types of filters, i.e., flat filters and bowtie filters, are usually employed to reduce patient dose. The flat filters, typically made of aluminum or copper, are used to attenuate the X-ray spectrum uniformly across the entire field of view (FOV) to remove low-energy X-rays. The bowtie filters are employed to modify the intensity of the X-ray beam inside the FOV. The patient cross section is typically oval-shaped and the bowtie filter is designed to compensate for the variable path length of X-ray beam through the patient.

Several different collimators have been proposed to further reduce radiation dose in CBCT. For example, Chityala *et al.* [36] proposed a concept of region-of-interest (ROI) CT where only ROI is irradiated with high-dose X-rays while outside of ROI is irradiated at a lower dose. Moor *et al.* [37] added a zonal filter to the CBCT X-ray tube of the Elekta Synergy linear accelerator to produce an un-attenuated beam for a central "target zone" and a partially attenuated beam for an outer "set-up zone". By using such collimator, doses along the axis of rotation were reduced by up to 50% in both target and set-up zones. Contrast-to-noise ratio (CNR) increased by up to 15% in zonally filtered CBCT images compared to full-field images due to the reduced scatter signal from attenuated beam. Chen *et al.* [2] and Lai *et al.* [38] proposed to use a volume-of-interest (VOI) filter for breast

*Address correspondence to this author at the Department of Radiation Oncology, UT Southwestern Medical Center, Dallas, TX 75390, USA; Tel: 214-645-7635 Fax: 214-645-2885; E-mail: jing.wang@utsouthwestern.edu

CBCT. In this method, a filtering mask is inserted between the x-ray source and the breast during image acquisition and the mask has an opening to allow full x-ray exposure to be delivered to a preselected VOI and a lower exposure to the region outside the VOI. Cho *et al*. [39] proposed a ROI image reconstruction with intensity weighting in circular CBCT. A non-uniform filter is placed in the X-ray beam to create regions of two different beam intensities and the CT image is reconstructed by the region of interest backprojection-filtration (BFP) algorithm [40-42]. In this manner, regions outside the target area can be given a reduced dose but still visualized with a lower CNR.

Zhu *et al*. [43] proposed an patient setup protocol for radiotherapy based on partially blocked CBCT. In this method, a sheet of lead strips is inserted between the X-ray source and the scanned patient. From the incomplete projection data, only several axial slices are reconstructed and used in the image registration for patient set-up. Since the radiation is partially blocked, the dose delivered onto the patient is reduced by a factor of more than 6, with an additional benefit of reduced scatter signals. As compared to registration using the regular CBCT, the registration difference using the partially blocked CBCT is less than 1 mm in translation and less than 0.2 degrees in rotation. The same concept has also been used for CBCT scatter correction [44].

III. ITERATIVE IMAGE RECONSTRUCTION FOR CBCT FROM UNDERSAMPLED PROJECTION VIEWS

Dose reduction for CBCT can also be achieved to acquire data with a reduced number of projection views. Severe artifacts are presented in CT images if they are constructed by analytical FBP-type of algorithms. Recently, several iterative image construction algorithms [45-47] based on the compressed sensing theorem [48] have been under investigation to improve CT image quality from undersampled projection views. Chen *et al*. [45] proposed a prior image constrained compressed sensing (PICCS) technique to enhance image quality of dynamic CT from highly undersampled projection data sets. Sidky *et al*. [47] proposed a constraint total-variation minimization method for circular CBCT image reconstruction from limited projection data. Excellent results have been obtained in those strategies.

IV. NOISE REDUCTION ALGORITHMS FOR LOW MAS CBCT

A cost-effective approach to reduce the radiation dose delivered to patients during the CBCT procedure is to acquire CT projection data with a lower mAs protocol. The use of automatic exposure control (AEC) for helical CT has been offered by CT manufactures to manage patient dose, where the tube current is automatically adjusted both angularly around patient and along the z-axis [49-52]. On the other hand, using overall low mAs protocol can further reduce imaging dose significantly. Compared with the collimator-based approaches mentioned above, low mAs CBCT offers several advantages including: 1) no modification of current component of CBCT hardware; 2) higher duty-cycle of X-ray tube; and 3) longer X-ray tube life. However, a downside of low mAs protocol is that the quality of the projection data and the reconstructed CBCT image will be degraded dra-

matically due to excessive quantum noise during intensity measurements. To recover the image quality of resultant CBCT, many strategies have been proposed to reduce noise in low mAs CBCT. In this section we will summarize the recent efforts devoted to improve image quality of noisy low-dose CT. In particular, we will describe the strategy of statistics-based sinogram smoothing/restoration followed by analytical image reconstruction in details because it generates very promising results and maximizes computational efficiency.

IV.A. Low-Pass Filter During Image Reconstruction

Noise usually appears as high-frequency component in frequency domain. Conventionally, noise in CT is suppressed by using a low-pass filter to attenuate the high-frequency component of the projection data during image reconstruction. Meanwhile, high frequency component also contains information about the tissue edges in the image. A simple low-pass filter cannot differentiate edge information from noise. Thus, noise reduction using a low-pass filter will result in the loss of edges, which is not desirable for low-dose CT imaging.

IV.B. Local Characteristics-Based Edge-Preserving Filter

In an effort to preserve edge information during noise suppression, several edge-preserving filters [53-57] have been proposed to reduce noise in either CT projections or reconstructed CT images. This type of filters is usually based on local characteristics of the projection data elements or image voxels. Demirkaya [57] used the classical anisotropic diffusion filter to suppress noise in projection data of fan-beam CT. Xia *et al*. [56] applied partial diffusion equation (PDE) based denoising technique for breast CBCT at different steps along the reconstruction process, and found that denoising performs better when applied to the projection data than the reconstructed image. Hsieh [53] developed an adaptive trimmed mean filter to suppress streak artifacts resulting from excessive X-ray photon noise. In this method, a one-dimensional (1D) filter is designed such that its parameters are dynamically adjusted to adapt to the local noise characteristics of raw projection data. Similarly, Kachelriess *et al*. [54] proposed a generalized multi-dimensional adaptive filter that applies non-linear filtering in the detector row, view and the z-direction. Zhong *et al*. [55] presented a wavelet-based algorithm to suppress noise in the ramp-filtered projection data for breast CBCT images and dose can be reduced by up to 60% while maintaining clinically accepted image quality. Borsdorf *et al*. [58] reported a wavelet domain noise reduction algorithm in which the threshold for wavelet coefficient is determined through correlation analysis of two spatially identical CT images reconstructed from two sets of projection data.

IV.C. Statistics-Based Sinogram Smoothing/Restoration

More recently, statistics-based sinogram smoothing/restoration algorithms [59-63] have shown advantages in noise reduction and edge preservation for low-dose CT. This type of adaptive strategy tends to estimate the ideal or noise-free line integrals from the noisy measurements through maximizing a statistical (e.g., penalized likelihood) objective function. CT images are then reconstructed by an analytical
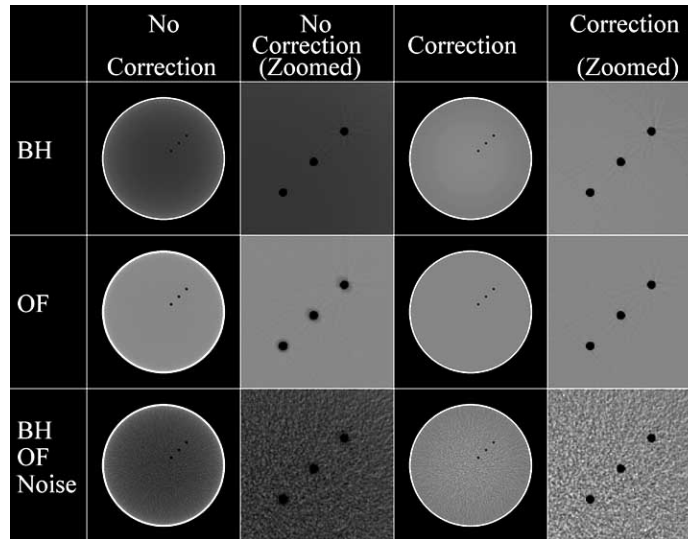
Fig. (1). Results of applying the sinogram restoration approach [64] to data corrupted with beam hardening alone (labeled BH), to data corrupted with off-focal radiation alone (labeled OF), and to data corrupted with both of these effects plus compound Poisson and electronic noise (labeled BH, OF, Noise). The left two columns involve reconstruction without correction for these effects and the right two columns after correction by the proposed penalized likelihood method with smoothing parameter 1.0. The window level is 0 HU and the width is 150 HU for all figures. (Figure reprinted with permission from La Riviere P.J *et al*, Penalized-likelihood sinogram restoration for computed tomography, *IEEE Transactions on Medical Imaging* 25, 1022-1036:2006. © 2006 IEEE).

reconstruction algorithm. The idea of this strategy is to retain the benefits of statistical modeling with the objective functions while avoiding the time consuming re-projection and back-projection cycle in the fully iterative statistical image reconstruction algorithms. The statistical objective function can be formulated according to statistical properties of either measured raw data or log-transformed projection/sinogram data. In the following sections, we will summarize these two different approaches for the estimation of ideal line integrals.

IV.C.1 Based on Statistics of Measured Raw Data

La Riviere *et al*. [61, 62, 64] proposed a strategy to estimate "ideal" line integrals based on the statistical properties of the measured raw data. Without considering polychromatic spectrum of X-ray photons, the measured signal I_i at detector bin *i* can be modeled as [62]:

$$I_i = \text{Poisson}(I_0 \exp(-l_i)) + \text{Normal}(0, \sigma_e^2) \qquad (1)$$

where l_i is the line integral along projection ray *i*, I_0 is the incident X-ray intensity and σ_e^2 is the variance of background electronic noise. When energy spectrum of X-ray photons is taken into account, the energy-weighted combination of Poisson random variable can be described by compound Poisson statistics [65, 66]. Because the sum of a compound Poisson distribution and a Gaussian distribution give rise to an intractable distribution, La Riviere [61] proposed to use an approximate statistical distribution of the measured raw data by approximating the compound Poisson distribution by a simple Poisson distribution and redefining new adjusted measurement. Then the ideal line integrals were estimated by maximizing a penalized Poisson-likelihood objective function [61, 64]. Fig. (**1**) shows the simulation results of the algorithm. The proposed algorithm outperforms the conventional low-pass filters as demonstrated by the noise-resolution curves in Fig. (**2**).

IV.C.2. Based on Statistics of Log-Transformed Projection Data

In the meantime, the noise model of the sinogram data after logarithm transform (i.e., line integrals) has been under investigation [60, 67], Wang *et al*. [67] performed a systematic experimental study on noise properties of low-dose CT projection data in the Radon space. An anthropomorphic torso phantom was scanned repeatedly by a Siemens CT scanner at five different mAs levels from 100 down to 17. The repeated measurements at each mAs level were used to test the normality of the repeatedly measured samples for each data channel using the Shapiro-Wilk test. The Shapiro-Wilk test gives the p-value for each of the repeated measurements at each channel. A smaller p-value indicates that the projection data at that channel is less likely to follow a normal distribution. The rejection percentage (those channels whose p-values are less than 0.05 divided by the total number of channels in each sinogram) for each mAs level is shown in Fig. (**3**). It can be observed that the rejection percentages increased from approximately 6% at 100 mAs level up to 9% at 17 mAs level for all data channels. This analysis indicates that even though the noise in low-dose projection data after logarithm transform cannot be approximated by a normal distribution, it is very close. Thus, a good candidate objective/cost function for calibrated low-dose sinogram data would be the penalized weighted least-squares (PWLS) criterion [63]. Mathematically, the PWLS cost function in sinogram domain can be written as:

$$\Phi(l) = \frac{1}{2}(\hat{y} - \hat{l})^T \Sigma^{-1}(\hat{y} - \hat{l}) + \beta R(l), \qquad (2)$$

where the first term is a weighted least-squares (WLS) criterion, $\hat{y}$ is the vector of the measured sinogram data, and $\hat{l}$ is the vector of ideal sinogram data to be estimated. Symbol *T* denotes the transpose operator. The matrix Σ is a diagonal
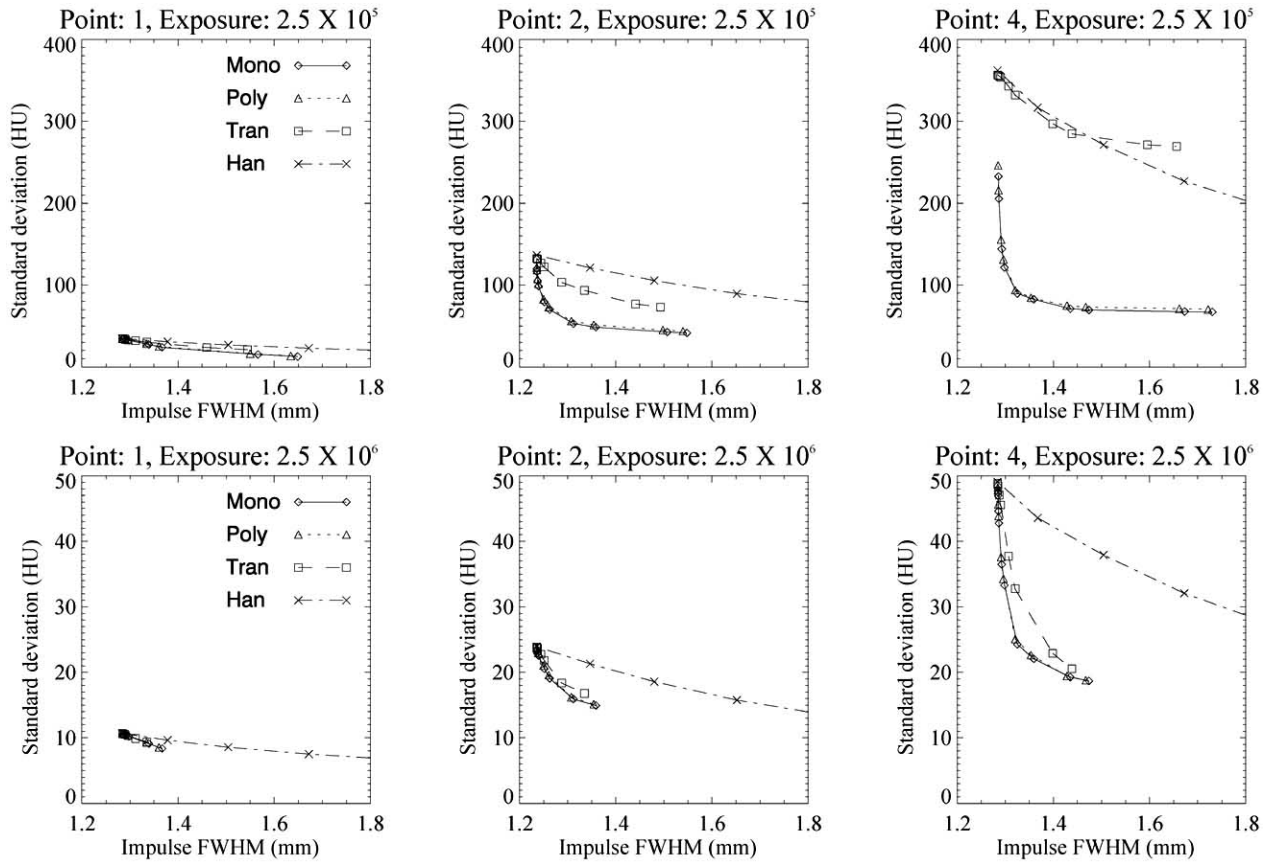
Fig. (2). Resolution-noise tradeoffs for exposures 2.5×105 and 2.5×106 at the center and right circular inserts in the ellipse phantom for the monochromatic line integral estimation approach (labeled "Mono"), the polychromatic line integral estimation approach (labeled "Poly"),the transmitted intensity estimation approach (labeled "Tran"), and conventional deconvolution followed by Hanning filtration (labeled "Han"). (Figure reprinted with permission from La Riviere P.J *et al*, Penalized-likelihood sinogram restoration for computed tomography, *IEEE Transactions on Medical Imaging* 25, 1022-1036:2006. © 2006 IEEE).
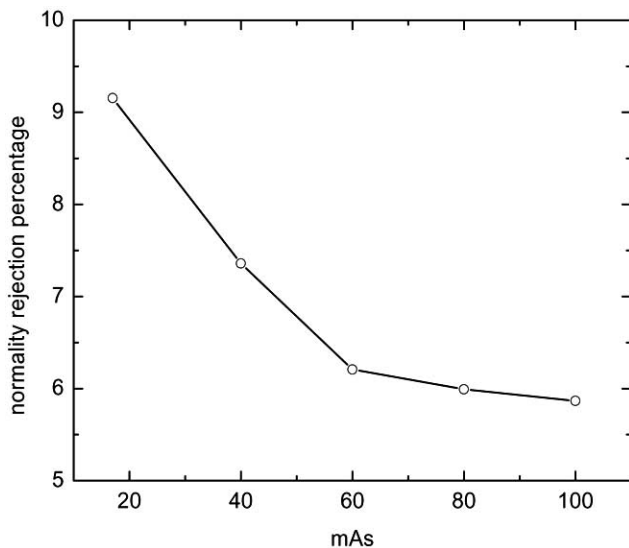

Fig. (3). Rejection percentage of the Shapiro-Wilk normality test for sinogram data at different mAs levels. (Figure reprinted with permission from Wang J. *et al*, 2008. An experimental study on the noise properties of x-ray CT sinogram data in Radon space, *Physics in Medicine and Biology* **53**, 3327-3341:2008).

matrix and its *i*th element is the variance of sinogram data at detector bin *i*. The second term in equation (2) is a smooth-

ness penalty or *a prior* constraint, where β is the smoothing parameter which controls the influence of the penalty. It is noted that PWLS cost function has been used in several medical imaging applications [68-70]. The key differentiation among these applications is the determination of the matrix Σ and the penalty term *R*.

The element of the diagonal matrix Σ is the variance of the corresponding sinogram datum and it determines the contribution of each sinogram datum to the cost function. Accurate estimation of the variance of each sinogram datum determines the performance of the PWLS criterion. From experimental studies [60, 67], it was found that variance of the sinogram datum can be estimated accurately by:

$$\sigma_i^2 = \exp(\tilde{l}_i) / N_{i0} , \qquad (3)$$

where N_{i0} is the incident photon number at detector bin *i*. To validate the above mean-variance relationship, the sample mean $\tilde{l}_i$ and variance σ_i^2 of each channel were calculated first from repeated scans, and then a comparison study was performed on the experimental sample variances calculated from the repeated scans with the theoretical variances predicted by equation (3). As shown in Fig. (**4**), good consistency between the variances calculated from repeated scans
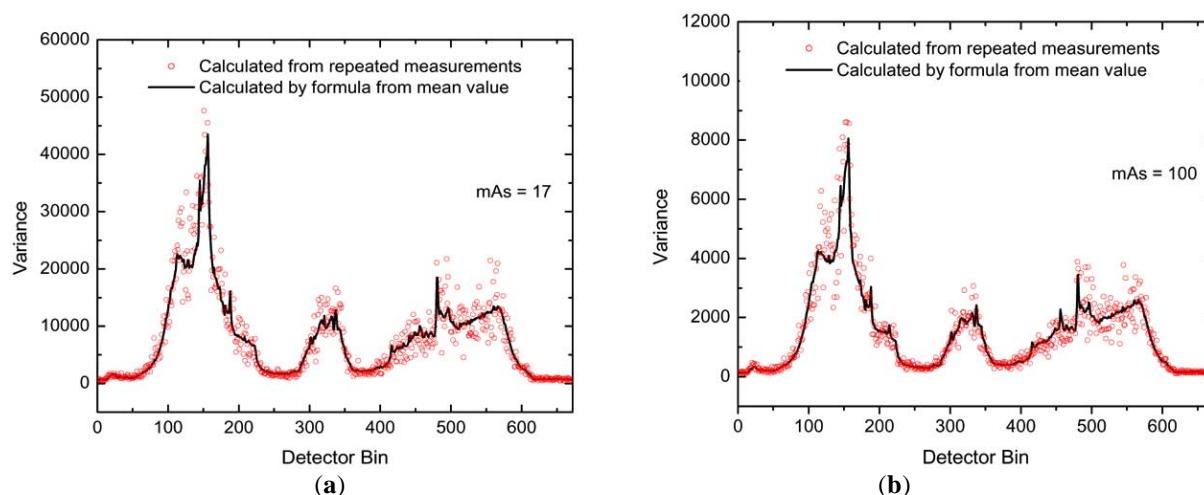
Fig. (4). Illustration of sinogram data variances calculated from repeated scans and from equation (3). (**a**)–result at 17 mAs, and (**b**)–result at 100 mAs. These variances from the repeated scans and from the prediction of equation (3) agree with each other very well. (Figure reprinted with permission from Wang J. *et al*, 2008. An experimental study on the noise properties of x-ray CT sinogram data in Radon space, *Physics in Medicine and Biology* **53**, 3327-3341:2008).

and from equation (3) is observed for both 17 and 100 mAs levels at an arbitrarily selected view.

According to equation (3), a sinogram datum with a larger mean value will have a larger variance and therefore less contribution to the cost function since the weight of that measured datum is $1/\sigma_i^2$, as defined in (2). This can be understood by the following observation. A larger sinogram datum value l_i at detector bin i indicates less X-ray photons being detected, i.e., smaller I_i in equation (1), or more photons being attenuated along the projection path i. A detector bin receiving less photons will be associated with a smaller signal-to-noise ratio (SNR) based on the Poisson noise nature of the detected X-ray photons. Therefore, the WLS criterion reflects the observation that the measured datum with a lower SNR will contribute less for the estimation of its ideal sinogram datum.

Another important factor that determines the performance of the PWLS criterion is the penalty term. In CT sinogram processing, a commonly used regularization takes a quadratic form with equal weights for neighbors of equal distance [60-63]. Such quadratic penalty simply encourages the equivalence between neighbors without considering discontinuities in the image and may lead to over-smoothing around sharp edges or boundaries. When the PWLS criterion was used to suppress noise in CBCT projection data, Wang *et al*. [71, 72] proposed an anisotropic quadratic penalty to consider the difference among neighbors of 2D projection data of CBCT. The coupling between neighbors should be smaller if the absolute value of difference between them is larger and this kind of neighbors should contribute less to the concerned solution. By such choice, the anisotropic quadratic-form penalty discourages the equivalence among neighbors if the gradient between them is large, and the edges or boundaries in the image could be better preserved.

The PWLS-based algorithm [71, 72] for noise reduction in low-dose CBCT was tested on a quality assurance phantom and an anthropomorphic head phantom. Fig. (**5**) shows one slice of the retained image containing several strips with

different sizes and contrasts. The CT image reconstructed by FDK [73] algorithm from the PWLS filtered sinogram obtained at 10 mA level is comparable to that at 80 mA. Fig. (**6**) shows the horizontal profiles along the central strips (see ROI1 of Fig. (**5c**)).

It can be observed that the edges are well preserved (as seen on the profiles through Fig. (**5b**) and (**5c**)) while noise is effectively suppressed (as seen from the profiles through Fig. (**5a**) and (**5b**)). Results of the anthropomorphic head phantom are shown in Fig. (**7**). It can be observed that noise in 10 mA CBCT images was efficiently suppressed after the sinogram was processed by the PWLS algorithm. The processed low-dose CT (10 mA) image was very similar to that of high-dose image (80 mA) by visual judgment. These phantom studies indicate that the imaging dose from CBCT can be reduced by a factor of 8 without loss of useful information for radiotherapy.

IV.D. Statistical Iterative Image Reconstruction

An alternative approach to reconstruction of low-dose CT images is to estimate attenuation coefficients iteratively by maximizing a penalized likelihood function that is constructed based on the noise statistics of the measurements. Compared with analytical reconstruction algorithms, a major advantage of iterative algorithms is that it considers the image physics, noise properties and imaging geometry elegantly. Advantages of iterative reconstruction algorithms have been demonstrated in the reconstruction of emission tomographic images [74-79]. However, when applying iterative reconstruction algorithms for CT imaging [80-83], long computational time may pose a challenge for their clinical applications. With the development of fast computers and dedicated hardwares [84, 85], iterative reconstruction algorithms may be used for clinical CT reconstruction in near future. Recently, iterative image reconstruction algorithms have demonstrated superior performance for reconstruction of the multi-slice helical CT [86] and cardiac micro-CT [87]. Efforts have also been devoted to investigate the use of iterative image reconstruction algorithm for noise reduction in
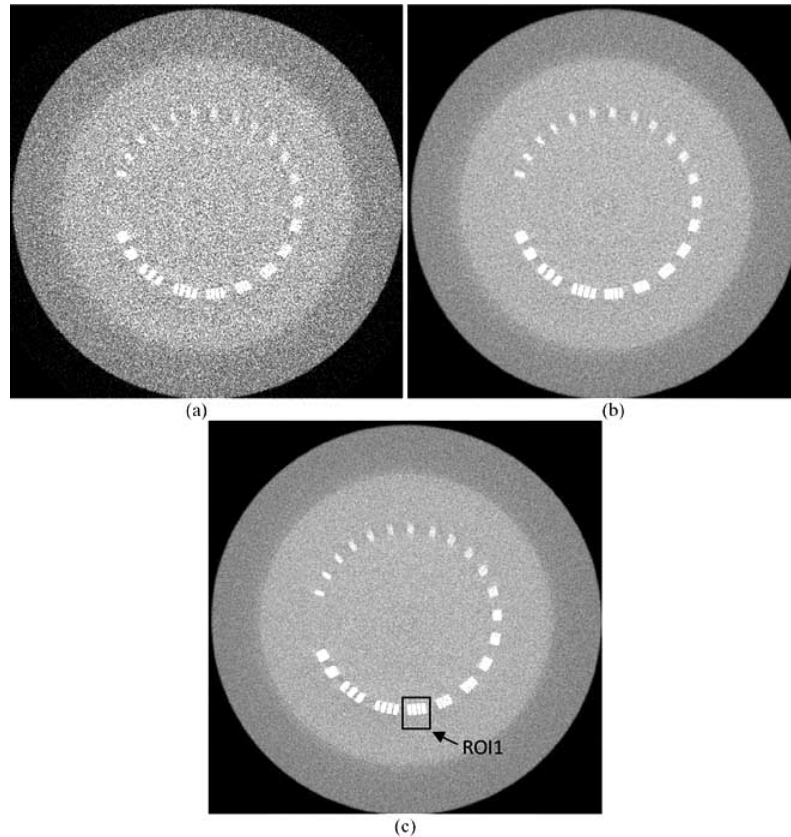
Fig. (5). One slice of FDK reconstructed image of the CatPhan® 600 phantom containing several strips: (**a**) from projection images acquired with 10 mA tube current; (**b**) after the sinogram of (**a**) was processed by the PWLS algorithm; and (**c**) from projection images acquired with 80 mA tube current. The duration of pulse of X-ray is 10 ms for both scans at 10 and 80 mA levels. (Figure reprinted with permission from Wang J. *et al*, 2008. Dose reduction for kilovoltage cone-beam computed tomography in radiation therapy, *Physics in Medicine and Biology,* **53**, 2897-2909:2008)
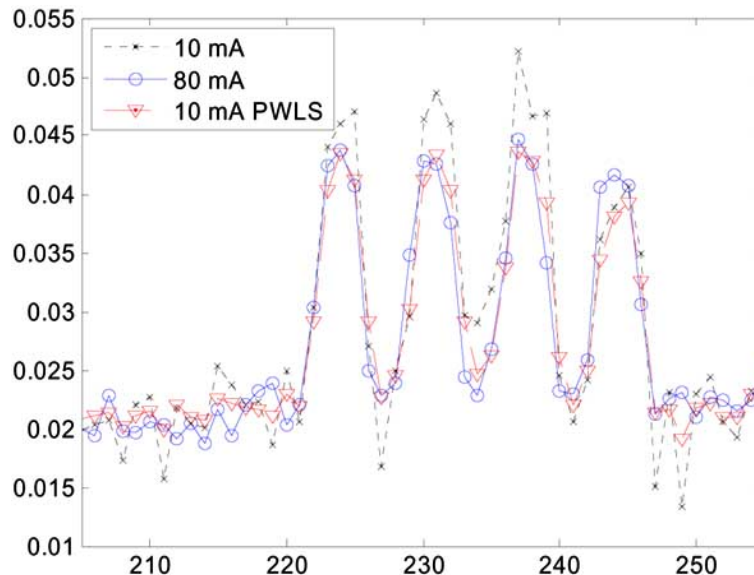

Fig. (6). Profiles though the central strips in Fig. (**5**) (indicated by ROI1). (Figure reprinted with permission from Wang J. *et al*, 2008. Dose reduction for kilovoltage cone-beam computed tomography in radiation therapy, *Physics in Medicine and Biology,* **53**, 2897-2909:2008).

low-dose CBCT. Wang *et al*. [88] proposed an iterative image reconstruction for low-dose CBCT based on the PWLS criterion with the edge-preserving penalty (discussed in section III.C.2). Results of this study are shown in Fig. (**8**). Fig. (**8a**) is the low-dose image reconstructed by analytical FDK algorithm and Fig (**8b**) shows the corresponding high-dose image reconstructed by the same FDK algorithm. It can be observed that the noise level is high in low-dose CBCT image. Fig. (**8c**) shows the low-dose image reconstructed by the iterative PWLS algorithm using isotropic quadratic penalty.
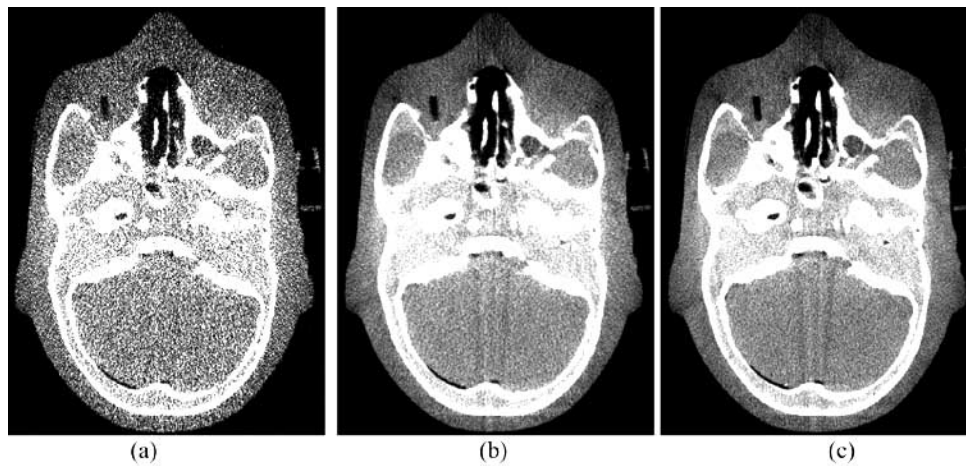
Fig. (7). One slice of FDK reconstructed image of the anthropomorphic head phantom: (**a**) from projection images acquired with 10 mA tube current; (**b**) after sinogram acquired with 10 mA tube current are processed by the PWLS algorithm; and (**c**) from projection images acquired with 80 mA tube current. (Figure reprinted with permission from Wang J. *et al*, 2008. Dose reduction for kilovoltage cone-beam computed tomography in radiation therapy, *Physics in Medicine and Biology,* **53**, 2897-2909:2008).
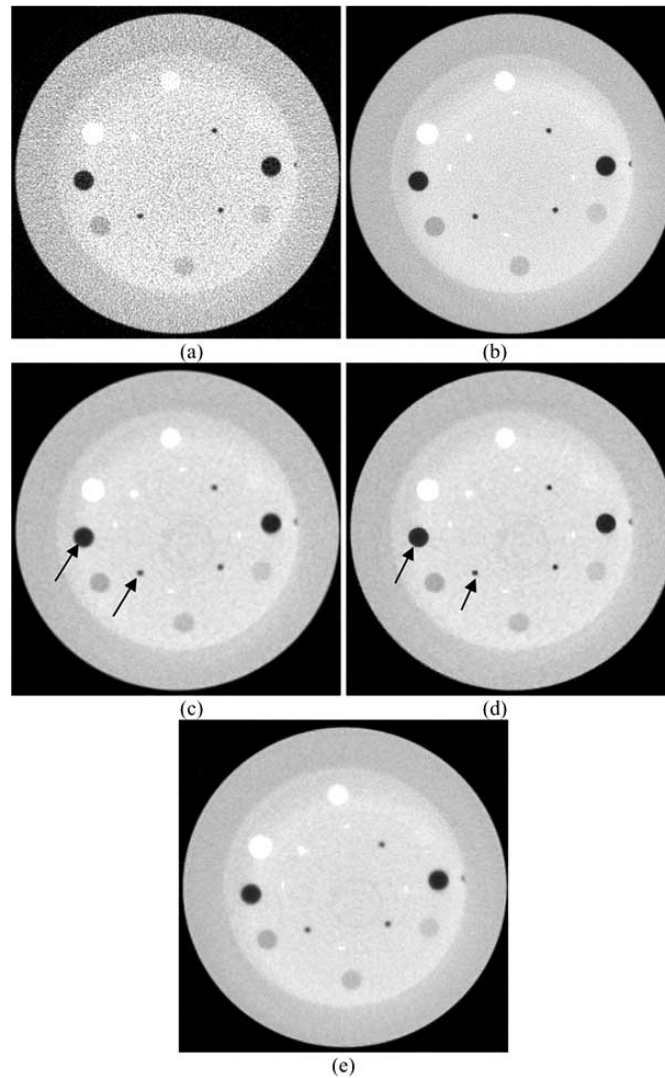

Fig. (8). CBCT of the CatPhan® 600 phantom: (**a**) analytical FDK reconstructed image from projection data acquired using low-dose protocol (10 mA/10 ms) and (**b**) high-dose protocol (80 mA/12 ms); (**c**) PWLS iterative image reconstruction with isotropic quadratic penalty from projection data acquired using low-dose protocol and (**d**) with the proposed anisotropic penalty; and (**e**) analytical FDK reconstructed image after low-dose projections processed by the PWLS criterion. (Figure reprinted with permission from Wang J *et al.*, 2009. Iterative image re-construction for CBCT using edge-preserving prior, *Medical Physics*, **36**, 252-260:2009).

Fig. **8**(**d**) displays the low-dose image reconstructed by the iterative PWLS algorithm using the edge-preserving anisotropic penalty. The noise in the images reconstructed by iterative algorithms is greatly suppressed as compared with that reconstructed using analytical method of Fig. (**8a**). While the edges were blurred in the low-dose image reconstructed by conventional isotropic penalty, the edges in the image reconstructed by edge-preserving penalty were better preserved, as indicated by arrows in Fig. (**8c**) and (**8d**). Fig. (**8e**) shows the result from the sinogram-domain smoothing [71] followed by analytical FDK reconstruction (described in section III.C.2). It can be observed that the edges in the image reconstructed by FDK from the PWLS processed projections are blurred compared with the image reconstructed by the iterative PWLS algorithm using the anisotropic quadratic penalty. This initial comparison study indicates that the edge-preserving penalty in image domain produces higher image resolution than the same penalty applied in projection domain at the cost of much longer computational time.

V. SUMMARY

Low-dose CBCT is desirable in clinical applications. CBCT dose reduction can be achieved by filtration or collimation of incident X-ray beams, reducing number of projection views and by the use of a low mAs protocol. To improve image quality of scans acquired at low mAs protocol, several strategies have been proposed to suppress noise including low-pass filter, local characteristics-based and statistics-based image processing and reconstruction algorithms. Among these noise reduction algorithms, the strategy of statistics-based projection smoothing/restoration plus analytical image reconstruction shows very promising results for dose reduction in CBCT. CBCT imaging dose can be reduced significant without compromising image quality by using these advanced noise reduction techniques.

ACKNOWLEDGEMENTS

REFERENCES

[1]   Chen B, Ning R. Cone-beam volume CT breast imaging: feasibility study. Med Phys 2002; 29: 755-70.
[2]   Chen L, Shaw CC, Altunbas MC, *et al.* Feasibility of volume-of-interest (VOI) scanning technique in cone beam breast CT--a preliminary study. Med Phys 2008; 35: 3482-90.
[3]   Gong X, Glick SJ, Liu B, Vedula AA, Thacker S. A computer simulation study comparing lesion detection accuracy with digital mammography, breast tomosynthesis, and cone-beam CT breast imaging. Med Phys 2006; 33: 1041-52.
[4]   Kwan AL, Boone JM, Shah N. Evaluation of x-ray scatter properties in a dedicated cone-beam breast CT scanner. Med Phys 2005; 32: 2967-75.
[5]   Ning R, Tang X, Conover D. X-ray scatter correction algorithm for cone beam CT imaging. Med Phys 2004; 31: 1195-202.
[6]   Gong X, Vedula AA, Glick SJ. Microcalcification detection using cone-beam CT mammography with a flat-panel imager. Phys Med Biol 2004; 49: 2183-95.
[7]   Ning R, Tang X, Conover D, Yu R. Flat panel detector-based cone beam computed tomography with a circle-plus-two-arcs data acquisition orbit: preliminary phantom study. Med Phys 2003; 30: 1694-705.
[8]   Xing L, Thorndyke B, Schreibmann E, *et al.* Overview of image-guided radiation therapy. Med Dosim 2006; 31: 91-112.
[9]   Groh BA, Siewerdsen JH, Drake DG, Wong JW, Jaffray DA. A performance comparison of flat-panel imager-based MV and kV cone-beam CT. Med Phys 2002; 29: 967-75.
[10]   Letourneau D, Wong JW, Oldham M, *et al.* Cone-beam-CT guided radiation therapy: technical implementation. Radiother Oncol 2005; 75: 279-86.
[11]   Cho PS, Johnson RH, Griffin TW. Cone-beam CT for radiotherapy applications. Phys Med Biol 1995; 40: 1863-83.
[12]   Siewerdsen JH, Jaffray DA. Cone-beam computed tomography with a flat-panel imager: magnitude and effects of x-ray scatter. Med Phys 2001; 28: 220-31.
[13]   Morin O, Gillis A, Chen J, *et al.* Megavoltage cone-beam CT: system description and clinical applications. Med Dosim 2006; 31: 51-61.
[14]   Jaffray DA, Siewerdsen JH. Cone-beam computed tomography with a flat-panel imager: initial performance characterization. Med Phys 2000; 27: 1311-23.
[15]   Jaffray DA, Siewerdsen JH, Wong JW, Martinez AA. Flat-panel cone-beam computed tomography for image-guided radiation therapy. Int J Radiat Oncol Biol Phys 2002; 53: 1337-49.
[16]   Ning R, Chen B, Yu R, Conover D, Tang X, Ning Y. Flat panel detector-based cone-beam volume CT angiography imaging: system evaluation. IEEE Trans Med Imaging 2000; 19: 949-63.
[17]   Baba R, Konno Y, Ueda K, Ikeda S. Comparison of flat-panel detector and image-intensifier detector for cone-beam CT. Comput Med Imaging Graph 2002; 26: 153-8.
[18]   Seppi EJ, Munro P, Johnsen SW, *et al.* Megavoltage cone-beam computed tomography using a high-efficiency image receptor. Int J Radiat Oncol Biol Phys 2003; 55: 793-803.
[19]   Baba R, Ueda K, Okabe M. Using a flat-panel detector in high resolution cone beam CT for dental imaging. Dentomaxillofac Radiol 2004; 33: 285-90.
[20]   Akpek S, Brunner T, Benndorf G, Strother C. Three-dimensional imaging and cone beam volume CT in C-arm angiography with flat panel detector. Diagn Interv Radiol 2005; 11: 10-3.
[21]   Pouliot J, Bani-Hashemi A, Chen J, *et al.* Low-dose megavoltage cone-beam CT for radiation therapy. Int J Radiat Oncol Biol Phys 2005; 61: 552-60.
[22]   Shaw C, Chen L, Altunbas M, *et al.* Cone beam breast CT with a flat panel detector-simulation, implementation and demonstration. Conf Proc IEEE Eng Med Biol Soc 2005; 4: 4461-4.
[23]   Glick SJ, Thacker S, Gong X, Liu B. Evaluating the impact of X-ray spectral shape on image quality in flat-panel CT breast imaging. Med Phys 2007; 34: 5-24.
[24]   Lai CJ, Shaw CC, Chen L, *et al.* Visibility of microcalcification in cone beam breast CT: effects of X-ray tube voltage and radiation dose. Med Phys 2007; 34: 2995-3004.
[25]   Sorensen S, Mitschke M, Solberg T. Cone-beam CT using a mobile C-arm: a registration solution for IGRT with an optical tracking system. Phys Med Biol 2007; 52: 3389-404.
[26]   Boone JM, Kwan AL, Seibert JA, Shah N, Lindfors KK, Nelson TR. Technique factors and their relationship to radiation dose in pendant geometry breast CT. Med Phys 2005; 32: 3767-76.
[27]   Liang Z, Lu H, Wen J, *et al.* Feasibility Studies on Low-dose Cone-beam 3D Mammography. Intl Conf Fully 3D Image Reconstruction in Radiology and Nuclear Medicine; Saint Malo, France: PM1-4, 2003.
[28]   Wen J, Lu H, Zhao W, Wang Z, Liang Z. A Study on Truncated Cone-beam Sampling Strategies for 3D Mammography. Conf Record IEEE NSS-MIC 2003; 5: 3200-4.
[29]   Yang Y, Schreibmann E, Li T, Wang C, Xing L. Evaluation of on-board kV cone beam CT (CBCT)-based dose calculation. Phys Med Biol 2007; 52: 685-705.
[30]   Lee L, Le QT, Xing L. Retrospective IMRT dose reconstruction based on cone-beam CT and MLC log-file. Int J Radiat Oncol Biol Phys 2008; 70: 634-44.
[31]   Lee L, Mao W, Xing L. The use of EPID-measured leaf sequence files for IMRT dose reconstruction in adaptive radiation therapy. Med Phys 2008; 35: 5019-29.

[32]   Brenner D, Hall E. Current concepts - Computed tomography - An increasing source of radiation exposure. N Engl J Med 2007; 357: 2277-84.

[33]   Islam M, Purdie T, Norrlinger B, *et al*. Patient dose from kilovolt-age cone beam computed tomography imaging in radiation therapy. Med Phys 2006; 33:1573-82.

[34]   Wen N, Guan H, Hammoud R, *et al*. Dose delivered from Varian's CBCT to patients receiving IMRT for prostate cancer. Phys Med Biol 2007; 52: 2267-76.

[35]   Murphy MJ, Balter J, Balter S, *et al*. The management of imaging dose during image-guided radiotherapy: Report of the AAPM Task Group 75. Med Phys 2007; 34: 4041-63.

[36]   Chityala RN, Hoffmann KR, Bednarek DR, Rudin S. Region of interest (ROI) computed tomography. Proc SPIE Med Imaging 2004; 5368: 534-41.

[37]   Moore CJ, Marchant TE, Amer AM. Cone beam CT with zonal filters for simultaneous dose reduction, improved target contrast and automated set-up in radiotherapy. Phys Med Biol 2006; 51: 2191-204.

[38]   Lai C-J, Chen L, Zhang H, *et al*. Reduction in x-ray scatter and radiation dose for volume-of-interest (VOI) cone-beam breast CT– a phantom study. Phys Med Biol 2009; 54: 6691-709.

[39]   Cho S, Pearson E, Pelizzari CA, Pan X. Region-of-interest image reconstruction with intensity weighting in circular cone-beam CT for image-guided radiation therapy. Med Phys 2009; 36: 1184-92.

[40]   Yu L, Zou Y, Sidky EY, Pelizzari CA, Munro P, Pan X. Region of interest reconstruction from truncated data in circular cone-beam CT. IEEE Trans Med Imaging 2006; 25: 869-81.

[41]   Zou Y, Pan X. Exact image reconstruction on PI-lines from minimum data in helical cone-beam CT. Phys Med Biol 2004; 49: 941-59.

[42]   Zou Y, Pan X, Sidky EY. Image reconstruction in regions-of-interest from truncated projections in a reduced fan-beam scan. Phys Med Biol 2005; 50: 13-27.

[43]   Zhu L, Wang J, Xie Y, Starman J, Fahrig R, Xing L. A patient set-up protocol based on partially blocked cone-beam CT. Technol Cancer Res Treat 2010; 9(2): 191-8.

[44]   Zhu L, Xie Y, Wang J, Xing L. Scatter correction for cone-beam CT in radiation therapy. Med Phys 2009; 36: 2258-68.

[45]   Chen G-H, Tang J, Leng S. Prior image constrained compressed sensing (PICCS): A method to accurately reconstruct dynamic CT images from highly undersampled projection data sets. Med Phys 2008; 35: 660-3.

[46]   Yu H, Wang G. Compressed sensing based interior tomography. Phys Med Biol 2009; 54: 2791-805.

[47]   Sidky EY, Pan X. Image reconstruction in circular cone-beam computed tomography by constrained, total-variation minimization. Phys Med Biol 2008; 53: 4777-807.

[48]   Candes EJ, Romberg J, Tao T. Robust uncertainty principles: exact signal reconstruction from highly incomplete frequency informa-tion. IEEE Trans Inform Theory 2006; 52: 489-509.

[49]   Gies M, Kalender WA, Wolf H, Suess C. Dose reduction in CT by anatomically adapted tube current modulation. I. Simulation stud-ies. Med Phys 1999; 26: 2235-47.

[50]   Kalender WA, Wolf H, Suess C. Dose reduction in CT by anatomi-cally adapted tube current modulation. II. Phantom measurements. Med Phys 1999; 26: 2248-53.

[51]   Mastora I, Remy-Jardin M, Delannoy V, *et al*. Multi-detector row spiral CT angiography of the thoracic outlet: dose reduction with anatomically adapted online tube current modulation and preset dose savings. Radiology 2004; 230: 116-24.

[52]   Mastora I, Remy-Jardin M, Suess C, Scherf C, Guillot JP, Remy J. Dose reduction in spiral CT angiography of thoracic outlet syn-drome by anatomically adapted tube current modulation. Eur Ra-diol 2001; 11: 590-6.

[53]   Hsieh J. Adaptive streak artifact reduction in computed tomogra-phy resulting from excessive x-ray photon noise. Med Phys 1998; 25: 2139-47.

[54]   Kachelriess M, Watzke O, Kalender W. Generalized multi-dimensional adaptive filtering for conventional and spiral single-slice, multi-slice, and cone-beam CT. Med Phys 2001; 28: 475-90.

[55]   Zhong J, Ning R, Conover D. Image denoising based on multiscale singularity detection for cone beam CT breast imaging. IEEE Trans Med Imaging 2004; 23: 696-703.

[56]   Xia JQ, Lo JY, Yang K, Floyd CE, Jr., Boone JM. Dedicated breast computed tomography: volume image denoising via a partial-diffusion equation based technique. Med Phys 2008; 35: 1950-8.

[57]   Demirkaya K. Reduction of noise and image artifacts in computed tomography by nonlinear filtration of the projection images. Proc SPIE Med Imag 2001; 4322: 917-23.

[58]   Borsdorf A, Raupach R, Flohr T, Hornegger J. Wavelet based noise reduction in CT-images using correlation analysis. IEEE Trans Med Imaging 2008; 27: 1685-703.

[59]   Li T, Schreibmann E, Thorndyke B, *et al*. Radiation dose reduction in four-dimensional computed tomography. Med Phys 2005; 32: 3650-60.

[60]   Li T, Li X, Wang J, *et al*. Nonlinear sinogram smoothing for low-dose X-ray CT. IEEE Trans Nucl Sci 2004; 51: 2505-13.

[61]   La Riviere P. Penalized-likelihood sinogram smoothing for low-dose CT. Med Phys 2005; 32: 1676-83.

[62]   La Riviere P, Billmire D. Reduction of noise-induced streak arti-facts in X-ray computed tomography through spline-based penal-ized-likelihood sinogram smoothing. IEEE Trans Med Imaging 2005; 24: 105-11.

[63]   Wang J, Li T, Lu H, Liang Z. Penalized weighted least-squares approach to sinogram noise reduction and image reconstruction for low-dose X-ray computed tomography. IEEE Trans Med Imaging 2006; 25: 1272-83.

[64]   La Riviere PJ, Bian JG, Vargas PA. Penalized-likelihood sinogram restoration for computed tomography. IEEE Trans Med Imaging 2006; 25: 1022-36.

[65]   Whiting B, Massoumzadeh P, Earl O, O'Sullivan J, Snyder D, Williamson J. Properties of preprocessed sinogram data in x-ray computed tomography. Med Phys 2006; 33: 3290-303.

[66]   Elbakri IA, Fessler JA. Statistical image reconstruction for polyen-ergetic X-ray computed tomography. IEEE Trans Med Imaging 2002; 21: 89-99.

[67]   Wang J, Lu HB, Liang ZR, *et al*. An experimental study on the noise properties of x-ray CT sinogram data in Radon space. Phys Med Biol 2008; 53: 3327-41.

[68]   Fessler JA. Penalized weighted least-squares image-reconstruction for positron emission tomography. IEEE Trans Med Imaging 1994; 13: 290-300.

[69]   Sukovic P, Clinthorne NH. Penalized weighted least-squares image reconstruction for dual energy X-ray transmission tomography. IEEE Trans Med Imaging 2000; 19: 1075-81.

[70]   Lu H, Li X, Hsiao I, Liang Z. Analytical noise treatment for low-dose CT projection data by penalized weighted least-square smoothing in the K-L domain. Proc SPIE Med Imaging 2002; 4682: 146-52.

[71]   Wang J, Li T, Liang Z, Xing L. Dose reduction for kilovoltage cone-beam computed tomography in radiation therapy. Phys Med Biol 2008; 53: 2897-909.

[72]   Zhu L, Wang J, Xing L. Noise suppression in scatter correction for cone-beam CT. Med Phys 2009; 36: 741-52.

[73]   Feldkamp L, Davis L, Kress J. Practical cone-beam algorithm. J Opt Soc Am A 1984; 1: 612-9.

[74]   Depierro AR. A modified expectation maximization algorithm for penalized likelihood estimation in emission tomography. IEEE Trans Med Imaging 1995; 14: 132-7.

[75]   Leahy RM, Qi JY. Statistical approaches in quantitative positron emission tomography. Stat Comput 2000; 10: 147-65.

[76]   Fessler JA, Hero AO. Penalized maximum-likelihood image-reconstruction using space-alternating generalized em algorithms. IEEE Trans Image Processing 1995; 4: 1417-29.

[77]   Li T, Thorndyke B, Schreibmann E, Yang Y, Xing L. Model-based image reconstruction for four-dimensional PET. Med Phys 2006; 33: 1288-98.

[78]   Liang Z, Hart H. Bayesian image-processing of data from con-strained source distributions - fuzzy pattern constraints. Phys Med-Biol 1987; 32: 1481-94.

[79]   Liang Z, Jaszczak R, Floyd C, Greer K, Coleman R. Bayesian reconstruction for SPECT: Validation with monte carlo simulation, experimental phantom, and real patient data. Int J Imag Syst Tech-nol 1989; 1: 149-68.

[80]   Beekman FJ, Kamphuis C. Ordered subset reconstruction for x-ray CT. Phys Med Biol 2001; 46: 1835-44.

[81]   Erdogan H, Fessler JA. Ordered subsets algorithms for transmis-sion tomography. Phys Med Biol 1999; 44: 2835-51.

[82]   Nuyts J, De Man B, Dupont P, Defrise M, Suetens P, Mortelmans L. Iterative reconstruction for helical CT: a simulation study. Phys Med Biol 1998; 43: 729-37.

[83]   Sauer K, Bouman C. A Local Update Strategy for Iterative Reconstruction from Projections. IEEE Trans Signal Process 1993; 41: 534-48.

[84]   Knaup M, Kalender WA, Kachelrieb M. Statistical Cone-Beam CT Image Reconstruction using the Cell Broadband Engine. IEEE Nucl Sci Symp Conf Rec 2006; 5: 2837-40.

[85]   Xu F, Mueller K. Accelerating popular tomographic reconstruction algorithms on commodity PC graphics hardware. IEEE Trans Nucl Sci 2005; 52: 654-63.

[86]   Thibault JB, Sauer KD, Bouman CA, Hsieh J. A three-dimensional statistical approach to improved image quality for multislice helical CT. Med Phys 2007; 34: 4526-44.

[87]   Song J, Liu QH, Johnson GA, Badea CT. Sparseness prior based iterative image reconstruction for retrospectively gated cardiac micro-CT. Med Phys 2007; 34: 4476-83.

[88]   Wang J, Li T, Xing L. Iterative image reconstruction for CBCT using edge-preserving prior. Med Phys 2009; 36: 252-60.